BACHELOR

Predicting photo-switching of cholesteric π-conjugated liquid crystals by means of Monte-Carlo simulations

Brils, Freek

Award date:
2018

Eindhoven University of Technology

Predicting photo-switching of cholesteric π-conjugated liquid crystals by means of Monte-Carlo simulations

Author:
Freek Brils

Supervisor:
Stefan Meskers

August 16, 2018

Summary

A Monte-Carlo model has been made to predict the photo-switching in cholesteric liquid crystals, giving more insight in these type of materials. This model is based on the work of Yang et. al[1] and numerically calculates the light transmitted through, reflected by and absorbed in a sample of a cholesteric liquid crystal. The model divides a the sample into several slabs which each act as a nematic liquid crystal. A randomly chosen slab randomly changes direction per iteration of the simulation. After several iterations, the total absorption in the crystal drops until it reaches a steady state. In this steady state, most absorption is present in the front of the slabs. This also resulted in the front of the slab having more variance in the angle between neighbouring slabs.

Contents

Chapter 1

Introduction

Opto-electronic devices such as light emitting diodes and solar cells play an important role in our society. Opto-electronic devices are devices which convert optical energy to electrical energy or vice-versa. Most of these devices are currently made out of inorganic materials. However, it is also possible to make opto-electronic devices from organic materials.

1.1 π-conjugated organic polymers

π-conjugated polymers are organic semiconductors that can be used in opto-electronic devices. The possibility of using π-conjugated polymers as semiconductors has gotten a lot of attraction in the past few decades. This interest resulted in several advances in the field of opto-electronics. Examples include organic light emitting diodes (OLEDs), organic field-effect transistors (OFETs) and lithium-ion batteries.

One of the main advantages of using organic opto-electronic devices is their production process. Inorganic devices are processed under high temperature and often expensive techniques such as molecular beam epitaxy.

The opto-electrical properties are influenced by the polymer structure. Often the light absorbed or emitted is polarized in a direction parallel to the polymer chain. Furthermore, side chains influence the charge carrier mobility. The π-π stacking distance can be increased by replacing linear side chains with more bulky alkyl branched side chains, influencing the supramolecular organization. This can result in an increase of hole mobility.

One well-known method of controlling the supramolecular organization is adding chirality to the polymer, often a liquid crystal. Chirality introduces new properties that can be measured. Examples are circular dichroism, optical rotary dispersion and electrochemical chiral sensing. Adding chirality can easily be done by adding chiral side chains to the polymer. This can also influence the opto-electrical properties as previously established.

Introducing this chirality into liquid crystals may create a helical organization of the molecules. A chiral liquid crystal is spatially periodic in one direction, normally chosen to be the z-axis. The length over which the average molecule orientation rotates a full 360°is called a pitch length. This pitch length depends on the structural molecule properties such as the monomer structure.

If the wavelength of incident light is comparable to this pitch length, strong Bragg scattering will occur[2].The light scattered this way is either circularly or elliptically polarized, depending on whether or not the incident light is parallel or oblique to the pitch direction.

Interesting monomers to use in such a liquid crystal are photo-switchable monomers. Photo-switchable monomer units change in structure when irradiated by light. A well-known example of this is the azobenzene molecule. When irradiated with light, this molecule changes from a trans-conformation to a cis-conformation. This can be seen in figure 1.1a. This isomerization is reversible.

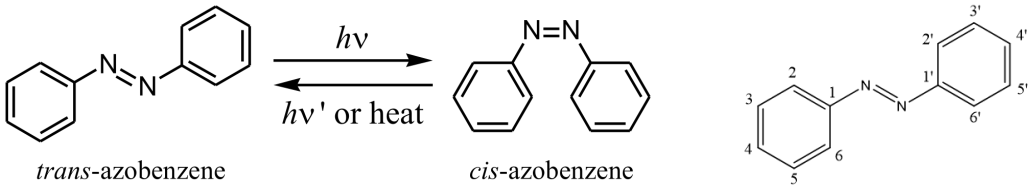

(a) Azobenzene's isomerization reaction under light influence, from trans-azobenzene to cis-azobenzene.

(b) Trans-azobenzene with numbered carbon-atoms.

Figure 1.1: Azobenzene and its multiple isomers

The impact of the isomerization can be illustrated by the change in distance between the C_4-$C_{4'}$ atoms (see figure 1.1b), which changes from roughly 9 to 6 Å in a trans-to-cis isomerization[3]. On top of that, an electric dipole is created after the isomerization.

It is clear that using photo-switch-able monomers in liquid crystals creates polymers which can be heavily influenced by incoming light. As early as 1971, Sackman showed that using azobenzene units inside polymers can be used to change the pitch length by means of photo-switch[4]. More recently, Rick Curvers synthesized a chiral fluorene-based copolymer at the Eindhoven University of Technology[5]. A photo-switchability was also shown in these polymers.

1.2 Aim of this Thesis

When continuously irradiating a photo-switchable chiral liquid crystal, its pitch length may change. It is expected that irradiating it with linearly polarized light will result in the molecules aligning with the light polarization, so that an steady state is reached where the minimum amount of light is absorbed. This is because the crystal layers which are out of this steady state will have a higher likelihood of getting photo-switched. These photo-switches will continue to occur until it is back in the previously established steady state. When irradiating a chiral liquid crystal with circularly or elliptically polarized light however, the system will be harder to predict.

This thesis focuses on predicting the behaviour of photo-switchable liquid crystals. This is done by numerically modeling a sample of cholesteric liquid crystals in Python. The numerical model is mainly based on the work of Deng-Ke Yang (2000)[1]. The sample will be modeled as several consecutive slabs with each its own Jones matrix. This Jones matrix can be used to calculate the reflection and transmission through this slab. Following this calculation, a random trans-cis or cis-trans isomerization will be imitated. This process will be executed several times to create a Monte-Carlo simulation. Both linearly, circularly and elliptically polarized light will be analysed.

The derivation and idea of the model is explained in the Theory section (chapter 2). Afterwards, the results will be analysed and discussed in the section Results (chapter 3). In the last part, a conclusion can be found.

Chapter 2

Theory

On a local scale, a cholesteric liquid crystal acts as a nematic liquid crystal. This means that the liquid crystal shows an oriental order in one direction; molecules are aligned parallel to each other, see figure 2.1a[2]. However, on a larger scale the liquid crystal is ordered helically. One can define a director $\hat{n}$ as the local direction the molecules are arranged in. For a cholesteric order, $\hat{n}$ rotates when moving along the z-axis and so overall the molecules are ordered in a helical arrangement:

$$n_x = cos(q_0 z + \phi) \tag{2.1a}$$

$$n_y = sin(q_0 z + \phi) \tag{2.1b}$$

$$n_z = 0. \tag{2.1c}$$

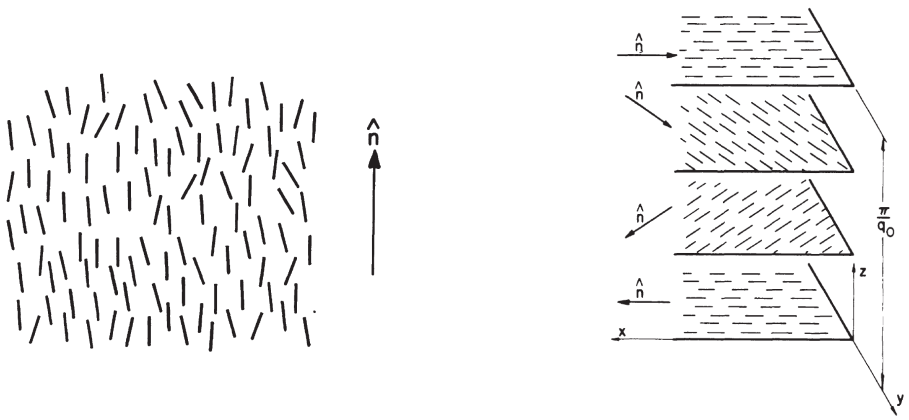

(a) The orientation of a polymer in a nematic phase. (b) The orientations of a polymer in a cholesteric phase.

Figure 2.1: Nematic and cholesteric order.

The pitch length can be calculated from these equations. This is the length for which the structure rotates a full 360°:

$$P = \frac{2\pi}{|q_0|}. \tag{2.2}$$

Now let us divide a sample into a number of N slabs, similar to figure 2.1b. If the sample has a thickness h, then the thickness of the slab is equal to $\Delta z = h/N$. Recall that orientation is locally nematic. Therefore, every slab has its own direction n_x, n_y, n_z. In a helical structure, the director of slab m and slab m+1 will have an angle equal to $\beta = \frac{2\pi}{P}\frac{h}{N}$.

2.1 Transmittance and reflectance calculation

Because the slabs are nematic, it is possible to derive a Jones matrix responsible for transmission of incoming light, and for reflection of incoming light. This can of course also be done for light coming from the opposite direction. This leads to the following equations for the electric field:

$$\vec{E}_{m,t} = \overleftrightarrow{A}_{(m+1)} \cdot \vec{E}_{(m+1),t} + \overleftrightarrow{B}_{(m+1)} \cdot \vec{E}_{(m+1),r} \tag{2.3a}$$

$$\vec{E}_{m,r} = \overleftrightarrow{C}_{(m+1)} \cdot \vec{E}_{(m+1),t} + \overleftrightarrow{D}_{(m+1)} \cdot \vec{E}_{(m+1),r}. \tag{2.3b}$$

In this formula, $\vec{E}$ is the Jones vector of light and subscript t and r represent light transmitted through and reflected by the material respectively. $\overleftrightarrow{A}$, $\overleftrightarrow{B}$, $\overleftrightarrow{C}$, and $\overleftrightarrow{D}$ represent the Jones matrices. Yang et al. showed that in this case they equal

$$\overleftrightarrow{A}_{(m+1)} = e^{i\delta_{(m+1)}} \times \begin{pmatrix} cos\beta_{(m+1)} e^{i\gamma_{(m+1)}} & -\frac{\overline{n}}{n_e} sin\beta_{(m+1)} e^{-i\gamma_{(m+1)}} \\ \frac{\overline{n}}{n_o} sin\beta_{(m+1)} e^{i\gamma(m+1)} & cos\beta_{(m+1)} e^{-i\gamma_{(m+1)}} \end{pmatrix} \tag{2.4a}$$

$$\overleftrightarrow{B}_{(m+1)} = \frac{\Delta n sin\beta_{(m+1)}}{2 n_e n_o} e^{-i\delta_{(m+1)}} \times \begin{pmatrix} 0 & -n_o e^{i\gamma_{(m+1)}} \\ -n_e e^{-i\gamma_{(m+1)}} & 0 \end{pmatrix} \tag{2.4b}$$

$$\overleftrightarrow{C}_{(m+1)} = \overleftrightarrow{B}^*_{(m+1)} \tag{2.4c}$$

$$\overleftrightarrow{D}_{(m+1)} = \overleftrightarrow{A}^*_{(m+1)}. \tag{2.4d}$$

In this case, $\delta_{(m+1)} = \frac{2\pi}{\lambda}\overline{n}\Delta z_{(m+1)}$ and $\gamma_{(m+1)} = \frac{\pi}{\lambda}\Delta n \Delta z_{(m+1)}$ where $\overline{n} = \frac{n_e + n_o}{2}$ is the average of the ordinary and extraordinary refraction index, and $\Delta n = n_e - n_o$ the difference.

Using these equations, it is possible to calculate the incoming light by normalizing the outgoing light as $E_{(N+1),t} = \begin{pmatrix} 1 \\ 0 \end{pmatrix}$ and the outoing light as $E_{(N+1),r} = \begin{pmatrix} 0 \\ 0 \end{pmatrix}$.

The problem with this method is that it is impossible to chose the incoming light. For example, the model cannot be used to find a prediction for an experiment using circularly polarized light as incoming light. Therefore, the following equations will be used,

$$\vec{E}_{(m+1),t} = \overleftrightarrow{J}_{abs} \cdot \overleftrightarrow{T}_t \cdot \vec{E}_{m,t} + \overleftrightarrow{J}_{abs} \cdot \overleftrightarrow{R}_r \cdot \overleftrightarrow{J}_{abs} \cdot \vec{E}_{(m+1),r} \tag{2.5a}$$

$$\vec{E}_{m,r} = \vec{\vec{R}}_t \cdot \vec{E}_{m,t} + \vec{\vec{T}}_r \cdot \vec{\vec{J}}_{abs} \cdot \vec{E}_{(m+1),r}. \tag{2.5b}$$

This defines the electric fields of the transmitted light and the reflected light at the end slab m, just before the interface between slab $m+1$. In this equation, J_{abs} is the absorption Jones matrix. T and R are the transmission and reflection Jones matrices respectively, with the subscript t and r indicating whether the matrices are for transmitting or reflecting light. Yang et. al showed that, when writing out the Jones matrices, these equations 2.5a and 2.5b equal:

$$\begin{aligned}\vec{E}_{(m+1),t} = {} & [e^{i\delta_{(m+1)}} \cdot \vec{\vec{M}}_{rot} \begin{pmatrix} e^{i\gamma_{(m+1)}} & 0 \\ 0 & e^{-i\gamma_{(m+1)}} \end{pmatrix}] \cdot \\ & [w \begin{pmatrix} cos\beta_{(m+1)} & \frac{\overline{n}}{n_e} sin\beta_{(m+1)} \\ -\frac{\overline{n}}{n_o} sin\beta_{(m+1)} & cos\beta_{(m+1)}] \end{pmatrix}] \cdot \vec{E}_{m,t} \\ & + [e^{i\delta_{(m+1)}} \cdot \vec{\vec{M}}_{rot} \begin{pmatrix} e^{i\gamma_{(m+1)}} & 0 \\ 0 & e^{-i\gamma_{(m+1)}} \end{pmatrix}] \cdot \\ & [w \frac{\Delta n}{2 n_e n_o} sin\beta_{(m+1)} \begin{pmatrix} \overline{n} sin\beta_{(m+1)} & n_o cos\beta_{(m+1)} \\ n_e cos\beta_{(m+1)} & -n_e sin\beta_{(m+1)} \end{pmatrix}] \cdot \\ & [e^{i\delta_{(m+1)}} \cdot \vec{\vec{M}}_{rot} \begin{pmatrix} e^{i\gamma_{(m+1)}} & 0 \\ 0 & e^{-i\gamma_{(m+1)}} \end{pmatrix} \cdot \vec{E}_{m,t}\end{aligned} \tag{2.6a}$$

$$\begin{aligned}\vec{E}_{m,r} = {} & [w \frac{\Delta n}{2 n_e n_o} \begin{pmatrix} \overline{n} sin\beta_{(m+1)} & -n_o cos\beta_{(m+1)} \\ -n_e cos\beta_{(m+1)} & -n_e sin\beta_{(m+1)} \end{pmatrix}] \cdot \vec{E}_{m,t} + \\ & [w \begin{pmatrix} cos\beta_{(m+1)} & -\frac{\overline{n}}{n_e} sin\beta_{(m+1)} \\ \frac{\overline{n}}{n_o} sin\beta_{(m+1)} & cos\beta_{(m+1)} \end{pmatrix}] \cdot \\ & [e^{i\delta_{(m+1)}} \cdot \vec{\vec{M}}_{rot} \begin{pmatrix} e^{i\gamma_{(m+1)}} & 0 \\ 0 & e^{-i\gamma_{(m+1)}} \end{pmatrix}] \cdot \vec{E}_{(m+1),r}.\end{aligned} \tag{2.6b}$$

In this calculation, $\vec{\vec{M}}_{rot}$ is the rotation matrix $\begin{pmatrix} cos\beta & -sin\beta \\ sin\beta & cos\beta \end{pmatrix}$. w is equal to $(cos^2\beta + \frac{\overline{n}^2}{n_e n_o} sin^2\beta)$.

It is also possible to calculate the electric field at the beginning of slab m, so immediately after the interface between $m-1$ and m. The transmitting light has not traveled through the slab at this point, so the J_{abs} has to be removed from equation 2.5a. The opposite is done for the reflecting light by adding a multiplication with J_{abs}. This results into

$$\vec{E}_{(m+1),t}|_m = \vec{\vec{T}}_t \cdot \vec{E}_{m,t} + \vec{\vec{R}}_r \cdot \vec{\vec{J}}_{abs} \cdot \vec{E}_{m,t} \tag{2.7a}$$

$$\vec{E}_{m,r}|_{(m-1)} = \vec{\vec{J}}_{abs} \cdot \vec{\vec{R}}_t \cdot \vec{E}_{m,t} + \vec{\vec{J}}_{abs} \cdot \vec{\vec{T}}_r \cdot \vec{\vec{J}}_{abs} \cdot \vec{E}_{(m+1),r} \tag{2.7b}$$

where $\vec{E}_{(m+1),t}|_m$ represents the transmitting electric field in slab $m+1$ at the interface between slab m.

This method has the advantage that the transmission can be calculated by arbitrarily choosing the incoming light instead of the outgoing light, instead of a reverse calculation. This however creates another problem. The set of equations do not allow the infinite reflections to be taken into account. In order to take it into account, equation 2.6 is calculated again for every slab. This is iterated multiple times until the transmittance in the last slab stops changing significantly.

2.2 Photo-switchable angle

The calculation from the previous section can predict the transmittance for a set of slabs. This of course does not include the photo-switchable effect. This effect changes the pitch length of the material by locally changing the polymer structure from trans to cis or vice-versa. Since the structure change is local, it is assumed that the effect can be simulated by changing the angle of the director of single slab. Therefore, a Monte-Carlo simulation will be executed.

It is not known which slab's angle will be changed. However, it can be assumed that the slab's chance to undergo isomerization is proportional to the energy absorbed by the slab and thus the absorbed intensity. The intensity can be calculated with

$$I_{m,t} = E_{x,m,t} \cdot E^*_{x,m,t} + E_{y,m,t} \cdot E^*_{y,m,t} \tag{2.8a}$$

for the transmitted light and

$$I_{m,r} = E_{x,m,r} \cdot E^*_{x,m,r} + E_{y,m,r} \cdot E^*_{y,m,r} \tag{2.8b}$$

for the reflected light.

Next, the absorption can be calculated:

$$I_{m,absorbed,t} = I_{m,t}|_{m-1} - I_{m,t}|_{m+1}, \tag{2.9a}$$

$$I_{m,absorbed,r} = I_{m,r}|_{m+1} - I_{m,r}|_{m-1}. \tag{2.9b}$$

These two can of course be added up to get the total absorption:

$$I_{m,absorped} = I_{m,absorbed,t} + I_{m,absorbed,r}. \tag{2.10}$$

The simulation will run several iterations in which every time one single director will change in angle by a value $\pm\Delta\beta$. As previously mentioned, every slab has a chance to be changed equal proportional to the intensity. This will be

$$P_m = \frac{I_{m,absorped}}{\sum_{m=1}^{N} I_{m,absorped}}. \tag{2.11}$$

After a slab has been chosen to change by a $\pm\Delta\beta$ it needs to be determined whether it has to be $+\Delta\beta$ or $-\Delta\beta$. This is however proportional to the prefered energy state, which would be the prefered molecule configuration. This is, regretfully, completely unknown. Therefore the best guess is to take $P_+ = 0.5$ and $P_- = 0.5$.

Chapter 3

Results and discussion

3.1 Steady state analysis

3.1.1 Linearly polarized light

First, the model was tested with linearly polarized light. The light incident is chosen to be $\frac{1}{2}\sqrt{2}\begin{pmatrix}1\\1\end{pmatrix}$, the $n_e = 1.8 + 0.008i$ and the $n_o = 1.5 + 1i$. Other used parameters can be found in the appendix A. After various amounts of angle changes, the absorption will drop. The reason for this is because one of the refractory index has a significantly smaller imaginary part. This can be seen in figure 3.1, which is an average of 50 simulations. At the end of the graph, the absorption barely changes anymore so it can therefore be concluded that a steady state is reached.

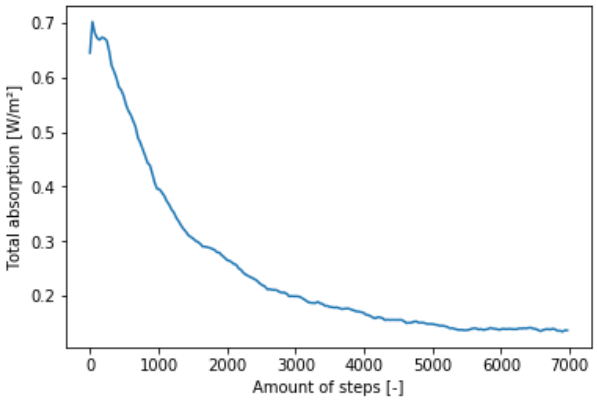

Figure 3.1: The total absorption in the sample as function of the amount of steps.

The average absorption per slab (1.5 nm) can be plotted against the position in the sample. This can be seen in figure 3.2. This can be compared to the initial absorption in figure in the same figure. It can clearly be seen that the absorption decreases as result of the photo-isomerizations. At the front of the sample, some light is still absorbed.

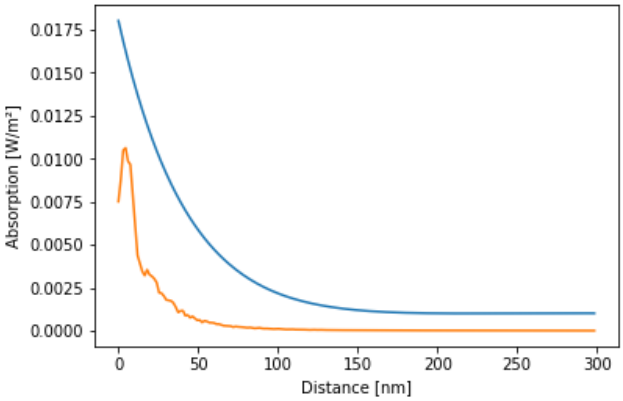

Figure 3.2: The average absorption per slab (1.5 nm) as a function of the z-axis after a steady state is reached. The blue line shows the initial absorption before any photo-isomarizations. The orange line shows the absorption after 7000 photo-isomerizations, which results in a steady state.

To see what happens within the structure, a plot is made of the angle between the directors in neighbouring slabs. This plot can be seen in figure 3.3. This plot includes three simulations which all have run until steady state is achieved. It can clearly be seen that the slabs align in such a way that the absorption is minimized. That is, the slabs at the end have an angle close to 0 radians or 2π radians. This will result in a nematic structure. At the start of the crystal, the slab orientates itself in the same direction as the light, which would be 45°and 45+180°, or $\frac{1}{4}\pi$ and $\frac{5}{4}\pi$. All three simulations in the graph and the majority of the simulations have their first value around these angles. After the first slab, the optimal polarization of light has not been reached for the next slab, so a this slab still needs a different angle with the previous one. This effect continues for a little while until around halfway through the slabs, around 150 nm.

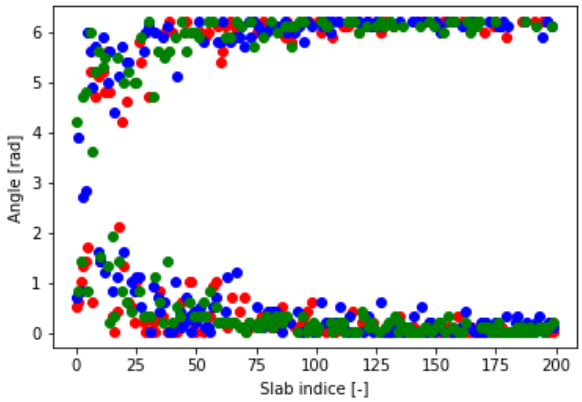

Figure 3.3: The distribution of the angle between the directors in neighbouring slabs as function of the slab index.

The average electric field transmitted through the sample is $\begin{pmatrix} 0.011 + 0.012i \\ -0.00073 + 0.0032i \end{pmatrix}$ and the

average of the electric field reflected by the sample is $\begin{pmatrix} -0.0024 - 0.094i \\ 0.0048 + 0.11i \end{pmatrix}$. The total intensity absorbed is 0.25 W/m^2, total intensity transmitted is 0.0013 W/m^2 and total intensity reflected is 0.022 W/m^2. This poses a problem since the sum of the transmitted, reflected and absorbed intensity is not equal to one, which is the intensity of the light before it reaches the sample.

Linearly polarized light in the form $\begin{pmatrix} 1 \\ 0 \end{pmatrix}$ is investigated too. A steady state has been reached in the simulation, as can be seen in figure 3.4. The initial absorption and steady state absorption can be seen in figure 3.5. It can easily be seen that this results in a similar steady state as the previously discussed linearly polarized light. A similar distribution of the angle can also be seen for this simulation in figure 3.6. The last slabs in the sample are all aligned around 0°even though the first isomerizations after initializing the simulation are more likely to happen in these slabs according to the initial absorption spectrum. For this polarization, the problem with the total intensity not adding up was also observed.

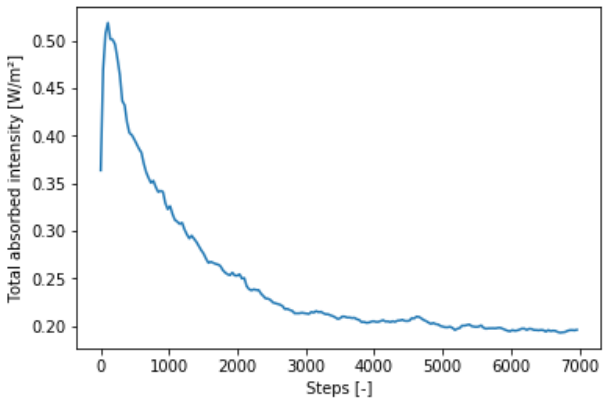

Figure 3.4: The total absorption as function of the amount of steps for $\begin{pmatrix} 1 \\ 0 \end{pmatrix}$ linear polarization.

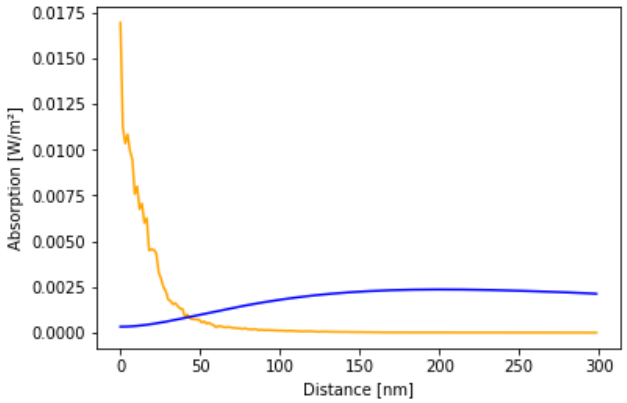

Figure 3.5: The average absorption as a function of the z-axis. The blue line shows the initial absorption before any photo-isomerizations for $\begin{pmatrix}1\\0\end{pmatrix}$ linear polarization. The orange line shows the absorption after 7000 photo-isomerization, which results in a steady state.

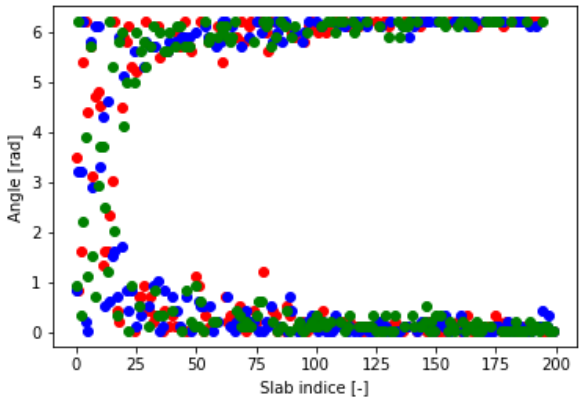

Figure 3.6: The distribution of the angle between the directors in neighbouring slabs as function of the slab index.

3.1.2 Circularly polarized light

A similar data analysis has been performed on circularly polarized light. The incident electric field of the light is $\frac{1}{\sqrt{2}}\begin{pmatrix}1\\ i\end{pmatrix}$. Steady state has been reached again as seen in figure 3.7. The average absorption against the position in the slab is plotted in figure 3.8. This shows a similar trend in the absorption as the final trend for the linearly polarized light. It turns out this is due to the same distribution in angle, as can be seen in figure 3.9. For this polarization, the same problem with the total intensity not adding up was observed.

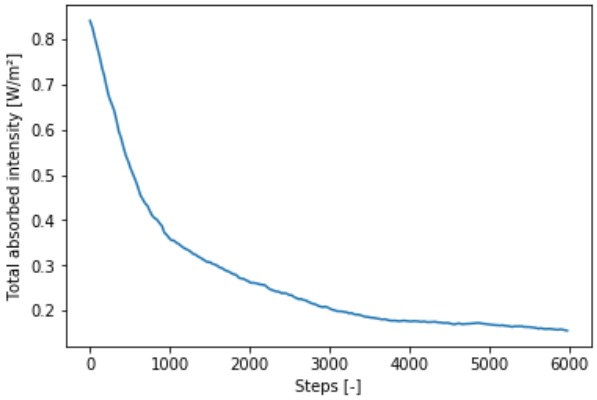

Figure 3.7: The total absorption as function of the amount of steps for elliptical polarization.

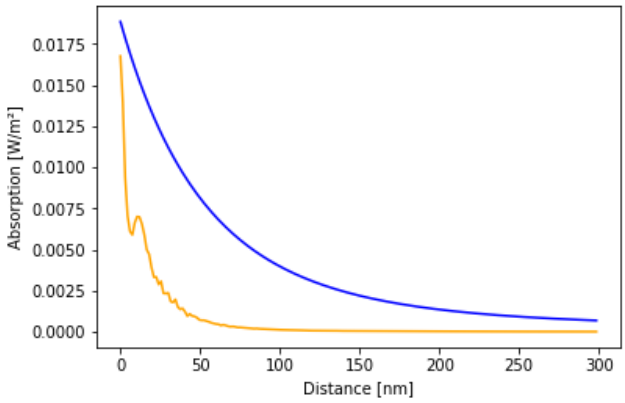

Figure 3.8: The average absorption as a function of the z-axis. The blue line shows the initial absorption before any photo-isomerizations for circular polarization. The orange line shows the absorption after 6000 photo-isomerizations are performed, which results in a steady state.

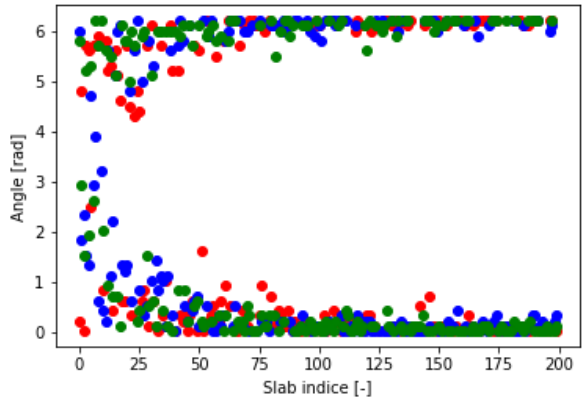

Figure 3.9: The distribution of the angle between the directors in neighbouring slabs as function of the slab index for circularly polarized light.

3.1.3 Elliptically polarized light

Elliptically polarized light has also been investigated. The polarization is $\begin{pmatrix} 0.44 + 0.42i \\ -0.76 + 0.24i \end{pmatrix}$. This results in the graphs shown in figure 3.10, 3.11 and 3.12. Steady state has been either been reached or almost reached by the end of the simulations.

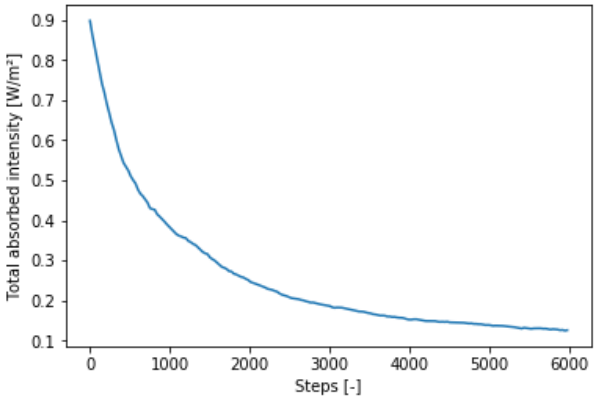

Figure 3.10: The total absorption as function of the amount of steps for elliptical polarization.

Figure 3.11 shows the same bulb in the absorption as the circularly polarized light. This suggests that this bulb is due to the rotating direction of the electric field in these polarizations. The light presumably rotates over the small distance where it reaches a suboptimal angle compared to the slab. No direct link between the slab distribution and this bulb can be found in figures 3.9 and 3.12.

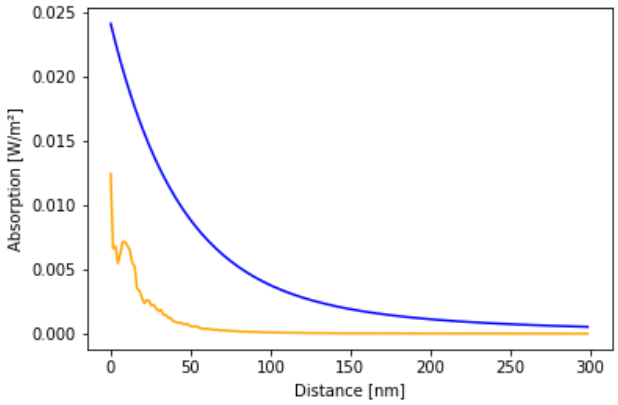

Figure 3.11: The average absorption as a function of the z-axis. The blue line shows the initial absorption before any photo-isomerizations for elliptical polarization. The orange line shows the absorption after 6000 photo-isomerization, which results in a steady state.

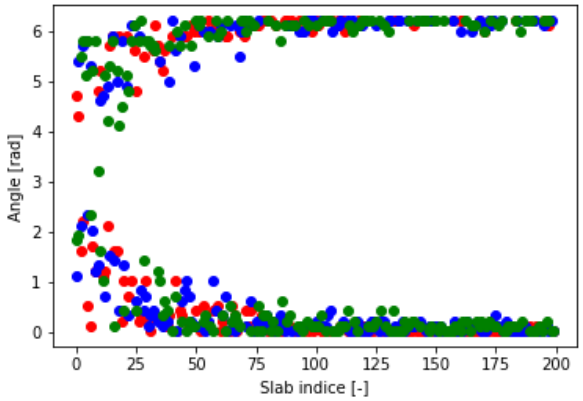

Figure 3.12: The distribution of the angle between the directors in neighbouring slabs as function of the slab index for elliptical polarization.

3.2 Analysis of transient evolution towards steady state

The evolution of the system towards the steady state has been analysed in order to understand why the angle distributions are the same for every polarization. It is expected that the similar angle distribution also has a similar origin. Because of the visually more different initial absorption compared to the other polarizations, $\begin{pmatrix}1\\0\end{pmatrix}$ linearly polarized light is investigated first. Roughly three areas can be distinguished in both figure 3.1 and 3.4. In the first relatively short area, the absorption does not decrease; most steps do not follow a trend. Afterwards the intensity decreases, presumably exponentially. At the very end, the absorption will barely change so the third and last part can be considered constant.

Several snapshots have been made after 200, 1000, 2000 and 4000 angle changes. The absorption spectrum of these can be seen in figure 3.13. The absorption becomes more sharp yet smaller as it moves towards the front of the sample.

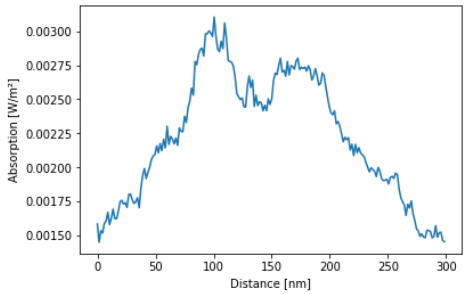

(a) The absorption of $\begin{pmatrix}1\\0\end{pmatrix}$ linearly polarized light after 200 angle changes.

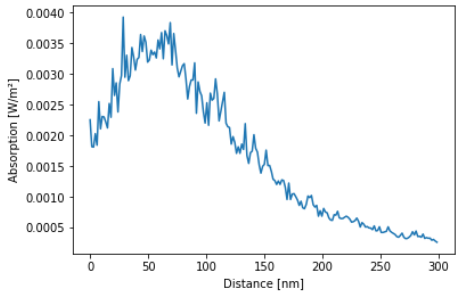

(b) The absorption of $\begin{pmatrix}1\\0\end{pmatrix}$ linearly polarized light after 1000 angle changes.

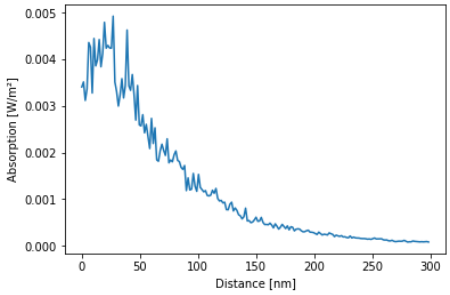

(c) The absorption of $\begin{pmatrix}1\\0\end{pmatrix}$ linearly polarized light after 2000 angle changes.

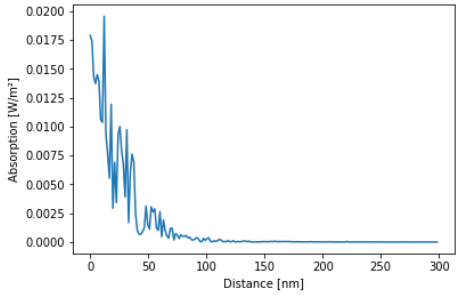

(d) The absorption of $\begin{pmatrix}1\\0\end{pmatrix}$ linearly polarized light after 4000 angle changes.

Figure 3.13: The absorption as function of the thickness through the slabs.

The slabs which angles are more heavily affected by the light also slowly move from the end of the slab to the beginning of the slab. This can be seen in figure 3.14. After 200 changes, no trend can be seen yet. A visual lack of a trend continues to exist until 2000 angle changes. From there on, it is apparent that the last quarter of slabs is settled; almost all of them have a director's angle around 0 or 2π radians, and the absorption is close to zero. The angled slabs slowly move

more to the right in figure 3.14d until it finds the very front of the sample. This results in the final accumulation seen in the figures in the previous sections.

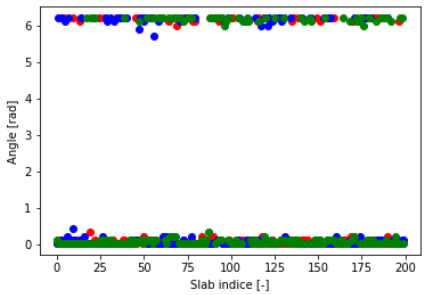

(a) The distribution of the angle between the directors in neighbouring slabs after 200 angle changes.

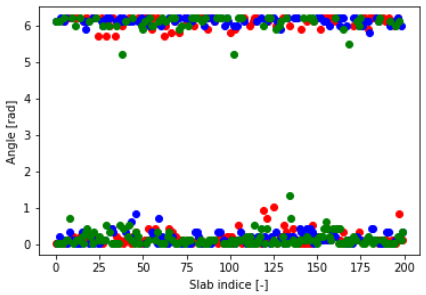

(b) The distribution of the angle between the directors in neighbouring slabs after 1000 angle changes.

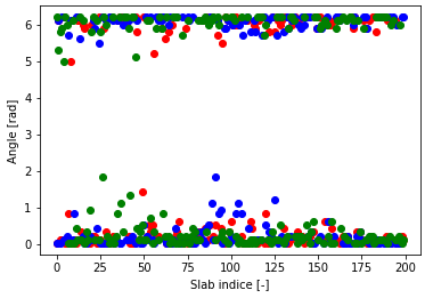

(c) The distribution of the angle between the directors in neighbouring slabs after 2000 angle changes.

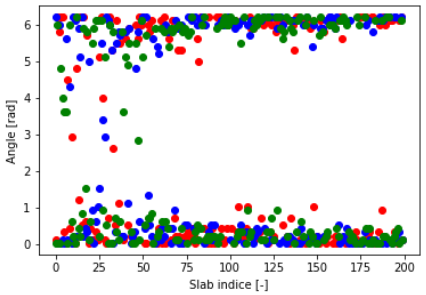

(d) The distribution of the angle between the directors in neighbouring slabs after 4000 angle changes.

Figure 3.14: The distribution of the angle between the directors in neighbouring slabs as function of the slab index through the sample.

It is expected that first the slabs at the higher absorption will change to a preferred angle. This results into a relatively higher change for the slabs in front of them to change. The slabs deeper in the sample will always have a smaller light intensity transmitting through them so the slabs in front of the previously changed section will start to become the most likely to change. Repeating this process will result in the peak in absorption slowly moving forward through the slab until it reaches the front of the sample.

One of the other things to note is that the final absorption through the slabs and the uncertainty in the angle between directors are related. This is possibly an exponentialy decreasing relation, which is similar to the absorption function for light transmitting through a simple material without taking polarization into account. It is proposed that this is related to each other: the structure of the sample will end up being nematic with the exception of the front of the sample. This part receives more light and thus will have more uncertainty in the director's direction.

All other light follows the same pattern, but starts at a later stage than the linearly polarized light, more similar to figure 3.14c.

3.3 Discussion

The Monte-Carlo simulations all progressed towards a steady state where the absorption in the sample is lower than the initial absorption in the sample. The behaviour of the sample is similar for all polarizations; linear, circular and elliptical. At the start slabs randomly change in angle slowly converting to a state in which the absorption is minimized. After a while, the absorption in the material will mainly be focused in the front of the material. It is expected that his comes from the higher intensity transmitting the sample at the front.

The model is not perfect of course so no hard conclusions can be drawn for the sample. One of the main problems with this model is that it does not take into account the structural preference of the liquid crystal. This makes it currently possible for a slab to rotate a full 360°. This movement is of course structurally hindered.

Next to that, some other mistakes have to be present in the simulation. This is proven by the fact that the total transmitted, reflected and absorbed intensity do not add up to the original intensity. On top of that, the formula provided by Yang et. al have been altered slightly. In the absorption matrix, the sign in the exponent has been changed from - to +. This is done because otherwise one will multiply with $e^{-i\delta} = e^{\frac{2\pi}{\lambda}(\overline{k}-i\overline{n}_{\mathbb{R}})\Delta z}$, which will increase the intensity as long as the imaginary part of the refractory index $n = n_{\mathbb{R}} + ik$ is positive. This is of course impossible. Next to that, the term $\frac{\overline{n}}{n_e}$ can be rewritten as $\frac{1}{2}(1 + \frac{n_o}{n_e})$. This term blows up if n_e approaches zero. The same is true for $\frac{\overline{n}}{n_o}$ with n_o approaching zero and $\frac{\Delta n}{2n_o n_e}$ with either one approaching zero. This can be prevented by assuming the n_o and n_e to be greater than one though. on top of that, a rotation matrix has been added to the absorption matrix.

Some results are still left unexplained. The absorbance initially rises for the linearly polarized light when starting the simulation. It is possible for it to be a random coincidence, even though it is an average of 120 simulations. In general, all analyses can have more simulations in order to smooth out the curves. On top of that, the change in angle per photo-isomerization is relatively big. This is done in order to reduce processing time, but it might be good practice to try smaller steps.

Conclusions and Outlook

A simulation tool for photo-switching of π-conjugated liquid crystalline polymers has been developed using the Monte-Carlo method. The simulations predict a spontaneous self-organization in the liquid crystal under illumination of light. This illumination results in the absorption being focused in the front of the sample, sometimes even absorbing more than the front slab absorbed before illumination. This way, the absorption in the other parts of the sample is minimized. This makes the total absorption in the sample drop. This reorganization is true for all tested polarizations, which include linear polarization, circular polarization and elliptical polarization.

Bibliography

[1] D.-K. Yang and X.-D. Mi, "Modelling of the reflection of cholesteric liquid crystals using the jones matrix," *Journal of Physics D: Applied Physics*, vol. 33, p. 672–676, March 2000.

[2] E. B. Priestley, P. J. Wojtowicz, and P. Sheng, *Introduction to liquid crystals*, ch. 1, pp. 5–7. Springer, 2013.

[3] H. L. Cheng, M. T. Tang, W. Tuchinda, K. Enomoto, A. Chiba, Y. Saito, T. Kamiya, M. Sugimoto, A. Saeki, and T. e. a. Sakurai, "Reversible control of radius and morphology of fluorene-azobenzene copolymer nanowires by light exposure," *Advanced Materials Interfaces*, vol. 2, no. 1, 2014.

[4] E. Sackmann, "Photochemically induced reversible color changes in cholesteric liquid crystals," *Journal of the American Chemical Society*, vol. 93, no. 25, p. 7088–7090, 1971.

[5] R. Curvers, "Photo-control on the chiroptical properties of a novel fluorene-based copolymer in solution and thin-film," Eindhoven University of Tehcnology, March 2018.

Appendix A

Appendix

The linear light was analysed with the following parameters:

Simulation	Polarization	Amount of Simulations
Linear	$\frac{1}{2}\sqrt{2}\begin{pmatrix}1\\1\end{pmatrix}$	50
Linear	$\begin{pmatrix}1\\0\end{pmatrix}$	70
Circular	$\frac{1}{\sqrt{2}}\begin{pmatrix}1\\i\end{pmatrix}$	120
Elliptical	$\begin{pmatrix}0.44+0.42i\\-0.76+0.24i\end{pmatrix}$	120

Parameter	Value	
Pitch length P	500	nm
Sample thickness h	300	nm
Number of slabs N	200	
Wavelength	500	nm
$\Delta\beta$	0.1	rad
Refraction index, ordinary n_o	1.5+1i	
Refraction index, extraordinary n_e	1.8+0.008i	